*J Mater Sci: Mater Electron* (2020) 31:17995–18003

# A comparative study of two-step and three-step methods for coating organometallic lead halide perovskite thin films

Sagar A. More[1], Rajendra Halor[1], Shaikh Raees[1], and Sanjay S. Ghosh[1,*]

[1] *Optoelectronics Laboratory, Department of Physics, Kavayitri Bahinabai Chaudhari North Maharashtra University, 425001 Jalgaon, Maharashtra, India*

**Received:** 9 April 2020
**Accepted:** 26 August 2020
**Published online:** 8 September 2020



## ABSTRACT

Two-step sequential spin coating deposition technique provides a cost-effective and high performance route for the synthesis of the organometallic lead halide perovskite materials. In this method, initially the metal halide film is coated, over which the MAI with a particular concentration is again spin-coated. However, it is difficult to obtain complete conversion of $PbI_2$ in $CH_3NH_3PbI_3$ perovskite. In this work, we show that good quality perovskite films can be coated by a three-step method to obtain improved conversion to perovskite and with improved materials properties. We have coated the perovskite films by two-step as well as three-step methods and presented a comparison of obtained film properties. Our results show that at lower concentration of MAI, complete conversion of $PbI_2$ does not take place. With increase in MAI concentration, in addition to the perovskite phase an intercalated MAI into $PbI_2$ phase is formed. In three-step coating, good phase of perovskite and improved morphology is obtained at comparatively lower MAI concentration. At higher concentrations of MAI in three-step method, leads to removal of already existing perovskite material and therefore leads to lower absorption.

## 1 Introduction

Due to ever increasing population, there is a tremendous hike in global energy demands. This has resulted in enhanced global energy dependence on fossil fuels, such as coal and petroleum. However, fossil fuels are not the permanent energy solution, and also it produces harmful effect on our environment due to toxic emissions [1–3]. Therefore, the scientific community is looking towards a suitable renewable energy source as a solution to future global energy needs. Among the renewable energy sources photovoltaic devices are one of the most promising alternatives. Due to high cost and energy intensive processes involved, well studied silicon technology is not being used widely [4]. Organic-

Address correspondence to E-mail: ssghosh@nmu.ac.in

https://doi.org/10.1007/s10854-020-04351-1

inorganic metal halide perovskite materials are the front runners in the search for low cost, solution processable and efficient photovoltaic devices. This comparatively new class of materials possesses excellent electrical and optical properties [5]. These are solution processable, flexible in terms of composition and can be deposited on the flexible substrates [6]. They combine the best properties of both inorganic as well as of organic materials [7].

Starting with 3.8% power conversion efficiency (PCE) in 2008, the perovskite solar cell performance has skyrocketed since then [8]. After a decade it has attained ~ 24% PCE in recent years [9]. They also have applications in light emitting devices (LEDs) [10], field effect transistors (FETs) [11], lasers [12], photo-detectors [13], etc. Two-step sequential deposition techniques provide cost-effective and high performance route for the synthesis of these materials. In this method, metal halide film is initially spin-coated. Over this, methyl ammonium iodide (MAI) is either spin-coated or dip-coated [14]. However, it is difficult to obtain complete conversion of $PbI_2$ in $CH_3NH_3PbI_3$ perovskite [15]. Also there is uncontrolled crystal growth and surface morphology [16].

Spin coating method has a significant role in the development of perovskite solar cells in a span of just a decade. Also commercialization by this method cannot be ruled out completely. In this account, we show that good quality perovskite films can also be coated by a three-step method to obtain improved materials properties. We have coated the perovskite films by two-step as well as three-step methods and presented a comparison of obtained film properties. Our results show that at lower concentration of MAI, complete conversion of $PbI_2$ does not take place. With increase in MAI concentration however intercalated MAI into $PbI_2$ phase is formed in two-step method. In three-step coating, good phase of perovskite and improved morphology is obtained at comparatively lower MAI concentration. At higher concentrations of MAI in three-step method leads to removal of already formed perovskite after the second step and therefore leads to lower absorption. The concentration of MAI solution is therefore critical in the final film properties of the film.

## 2 Experimental methods

MAI synthesis was performed by drop-wise addition of 10 ml of hydro-iodic acid (HI) (57 wt% in water, sigma Aldrich) in 24 ml of methyl amine (33 wt% in absolute ethanol, sigma Aldrich) [17]. Reaction was allowed at 0°C for 2 h. Precipitate was collected by drying the solution in rotary evaporator at 50°C. After collection of raw $CH_3NH_3I$, purification was performed by re-dissolving in 80 ml ethanol and again precipitated with the addition of 300 ml diethyl ether. The purification process was repeated twice and final $CH_3NH_3I$ was collected after drying in vacuum oven at 60°C for 24 h. Perovskite synthesis was performed using two-step and three-step sequential deposition spin coating methods. In two-step method, initially $PbI_2$ (461 mg/ml in DMF) layer was coated on glass substrate followed by thermal annealing at 100°C for 5 min. After cooling down the $PbI_2$-coated substrates, MAI layer was spin-coated at 1000 rpm on it, followed by annealing at 100°C for 5 min. The concentration of MAI was varied as 10, 20, 30 and 40 mg/ml, while other parameters were kept constant. In three-step, we followed same methodology as in two-step, only an additional MAI layer deposition was performed followed by annealing at 100°C for 5 min. Schematic diagram of the two processes is shown Fig. 1.

To record the UV-Visible absorption spectra, spectrophotometer (UV 1600) from Shimadzu was used. Morphology of the films were studied using scanning electron microscope (S-4800) from Hitachi. X-ray diffractometer (D8 advance Bruker) with incident source wavelength $\lambda = 1.54$ Å in coupling mode was used to record the x-ray diffraction (XRD) spectra for identification of the material phase and crystallinity. Raman spectra were recorded using (RenishawInVia microscope Raman, Resolution 1 $cm^{-1}$, excitation source 633 nm line of He-Ne laser). Thickness and roughness measurements were performed using Dektak-150 Profilometer.

## 3 Results and discussion

$PbI_2$ films were coated using the method described above. The UV-Visible absorption spectra, scanning electron microscopy image, XRD and the Raman spectra of the film is shown in Fig. 2. The UV-Visible absorption spectroscopy results of the perovskite film

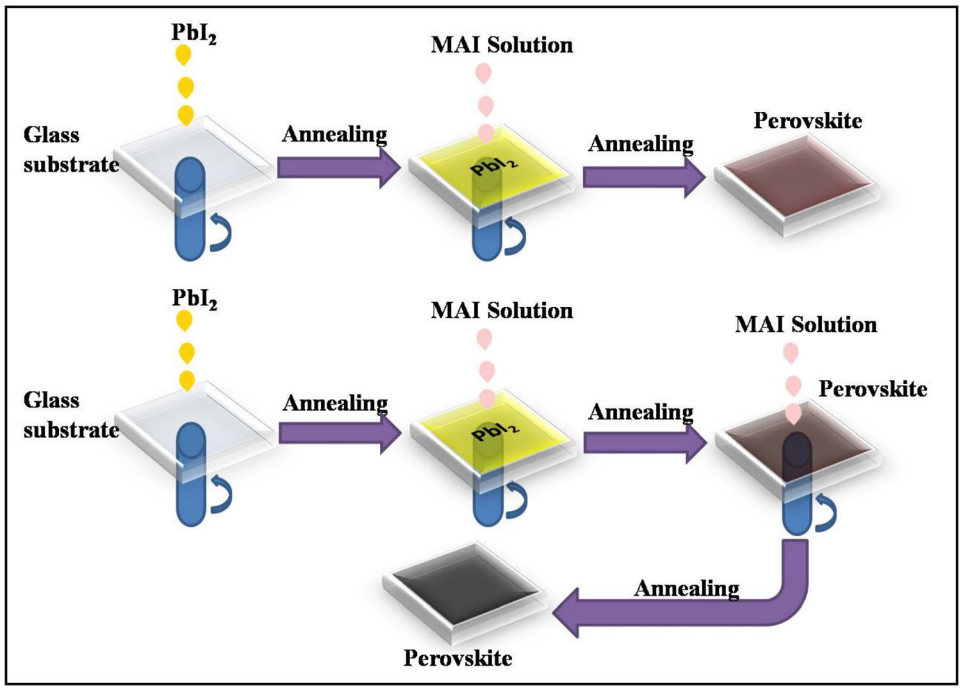


**Fig. 1** Schematic diagram showing the perovskite film deposition process by two and three-step methods

coated by two- and three-step methods with different concentrations of MAI are shown in Fig. 3. Photographs of the corresponding films are also shown. The results show absorption onset at 520 nm for the $PbI_2$ film and ~ 780 nm for all perovskite samples. Insets show the corresponding plot with energy on the x-axis. The optical bandgap was calculated using the relation.

$$E_g = {}^{hc}/_{\lambda_{ab}},$$

where $h$ is the planks constant, $c$ is the speed of light in vaccum and $\lambda_{ab}$ is the absorption onset. The calculated value of optical bandgap is ~2.38 eV for the $PbI_2$ film and ~1.58 eV for all the perovskite samples prepared by two- and three-step methods. The absorption onset and the calculated optical bandgap values matches with the reported values of perovskite $CH_3NH_3PbI_3$, which confirms the formation of perovskite phase by both two-step and three-step methods [18]. Few reported values of bandgap have been compared with the values obtained in the present study in Table 1.

In case of two-step method, absorption spectra show rise in absorption coefficient with decreasing wavelength below the absorption edge. At 10 mg/ml concentration, in addition to the perovskite absorption onset a distinct absorption kink at 520 nm was observed. Peak at 520 nm belongs to $PbI_2$ absorption. This indicates that there may be presence of some amount of $PbI_2$ in the film, along with the formed perovskite material. With 20 mg/ml and higher concentrations of MAI, the distinct clear kink at 520 nm was not observed, indicating better conversion of $PbI_2$ into perovskite phase. However, absorption below 520 nm still increases and reaches maximum at 440 nm similar to that of $PbI_2$ which indicates the presence of $PbI_2$ phase. In case of three-step method, absorption spectra show rise in absorption coefficient with decreasing wavelength beyond the absorption edge, but no distinct kink at 520 nm was observed for concentrations above 10 mg/ml. This indicates better perovskite phase formation from $PbI_2$ at lower concentrations of MAI. For 30 mg/ml and 40 mg/ml films, however, a distinctive kink at 580 nm was observed. Absorption feature at 580 nm is attributed to the intercalation state of MAI and $PbI_2$. It is considered a red-shifted and broadened $PbI_2$-like absorption [22].

The XRD patterns for two-step-coated films with varying concentrations of MAI over $PbI_2$ layer are shown in Fig. 4a. The sample coated with 10 mg/ml concentration of MAI shows the formation of perovskite phase (prominent diffraction peaks at 14.2 and 28.6 values of $2\theta$) [15, 23, 24]. In addition, peaks (at 12.7, 25.5, 38.8 values of $2\theta$) corresponding to $PbI_2$

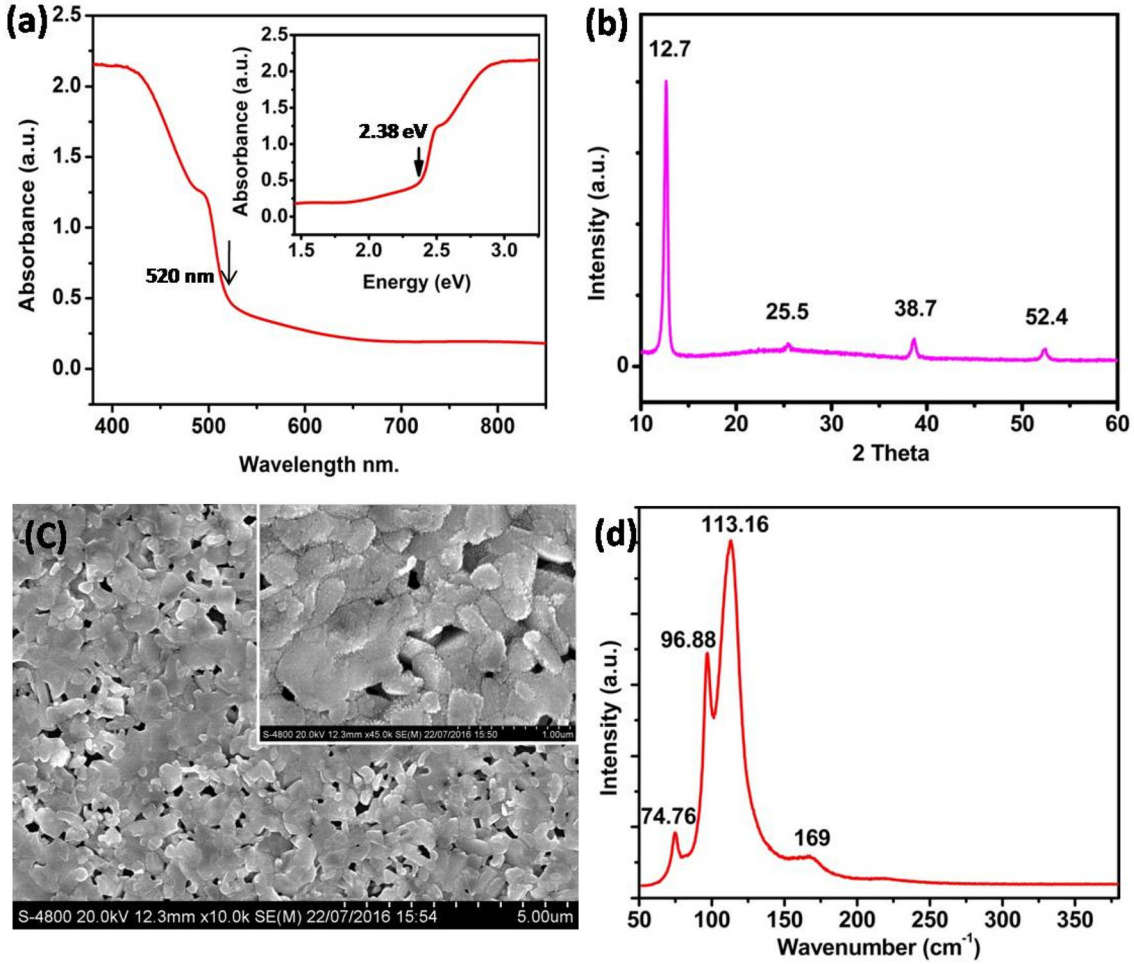


**Fig. 2** **a** Absorption spectrum, **b** XRD spectrum, **c** SEM image and **d** Raman spectrum of spin-coated $PbI_2$ film

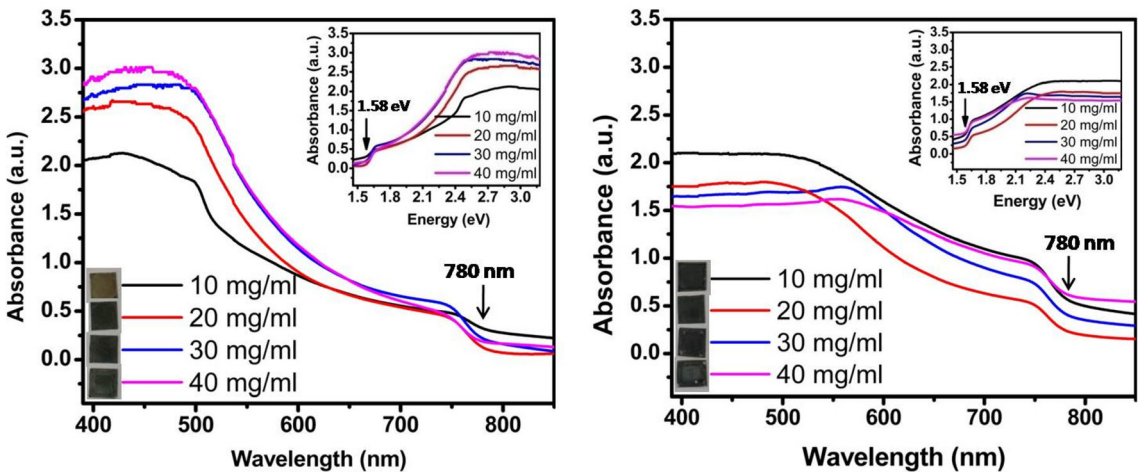


**Fig. 3** Absorption spectra of the films coated by **a** two-step and **b** three-step methods. Inset contains the respective plot in eV on x-axis. Photographs of the corresponding films are also shown

**Table 1** Reported values of optical bandgap have been compared with the values obtained in the present study

| Material | Bandgap values reported in the literature (eV) | Bandgap values obtained in the present study (eV) |
|---|---|---|
| $PbI_2$ | 2.36 [19] | 2.38 |
| $CH_3NH_3PbI_3$ deposited by spin coating | 1.55 [20] | 1.58 |
| $CH_3NH_3PbI_3$ deposited by vacuum method | 1.58 [21] | – |

are also seen [23–25]. This shows that complete conversion of $PbI_2$ into perovskite phase has not taken place in the film. As the concentration of MAI is increased to 20 mg/ml, the peak intensity at 12.7 value of $2\theta$ decreases, indicating a better conversion of $PbI_2$ phase. For 30 mg/ml concentration of MAI, intensity of peak at 12.7 reduces further as compared to that at 14.2. This shows further reduction in $PbI_2$ phase compared to the perovskite phase. Along with the above trend, a new peak at 11.6 degree appears for the film with 20 mg/ml concentration of MAI, the intensity of which enhances with increase in MAI concentration. This peak is attributed to the intercalation of MAI into $PbI_2$ [26]. For 40 mg/ml concentration of MAI, the peak at 12.7 degree corresponding to $PbI_2$ phases vanishes nearly completely but with enhanced intensity of the peak at 11.6 degree. Significant change in the intensity of peak at 14.2 value of $2\theta$ was not observed. This shows that with increasing MAI concentration, no enhancement in perovskite phase formation was obtained. The increased MAI in the film leads to the formation of intercalated methyl ammonium into the lead iodide. XRD spectra of the films coated with three-step method are shown in Fig. 4b. With 10 mg/ml concentration of MAI, the perovskite film shows features similar to that of film coated using 10 mg/ml with two-step method. The high intensity at 12.7 degree compared to 14.2 degree shows the dominance of $PbI_2$ phase over the perovskite phase. With 20 mg/ml concentration of MAI, the peak corresponding to $PbI_2$ is much reduced as compared to the perovskite peak at 14.2 degree, indicating the better conversion of $PbI_2$ into perovskite. This is better perovskite formation as compared to the film coated with the same concentration using two-step coating method. With 30 mg/ml concentration of MAI, further reduction of $PbI_2$ phase was observed but with enhanced intensity of peak at 11.6 degree. As the concentration of MAI was increased to 40 mg/ml, the intensity of peak at 14.2 degree corresponding to perovskite reduces indicating reduced perovskite phase available for X-ray diffraction.

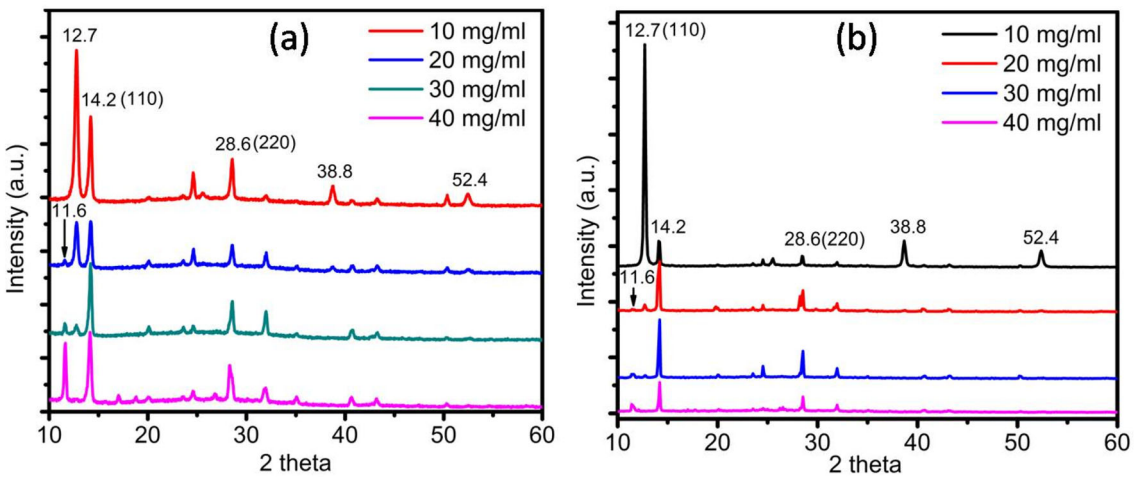


**Fig. 4** XRD spectra of the films coated by **a** two-step and **b** three-step methods

In order to study the morphology of film coated through two-step and three-step methods, scanning electron microscopic (SEM) images were recorded (Fig. 5). The morphology of the perovskite thin film obtained via sequential deposition methods was greatly influence by concentration MAI solution. In Two-step 10 mg/ml MAI concentration film, morphology shows hexagonal-shaped particles having diameter of 0.2–0.3 micrometer. These particles are in agglomerated form or are partially connected with each other. Along with these few particles with flake-like structure of length over one micrometer are also

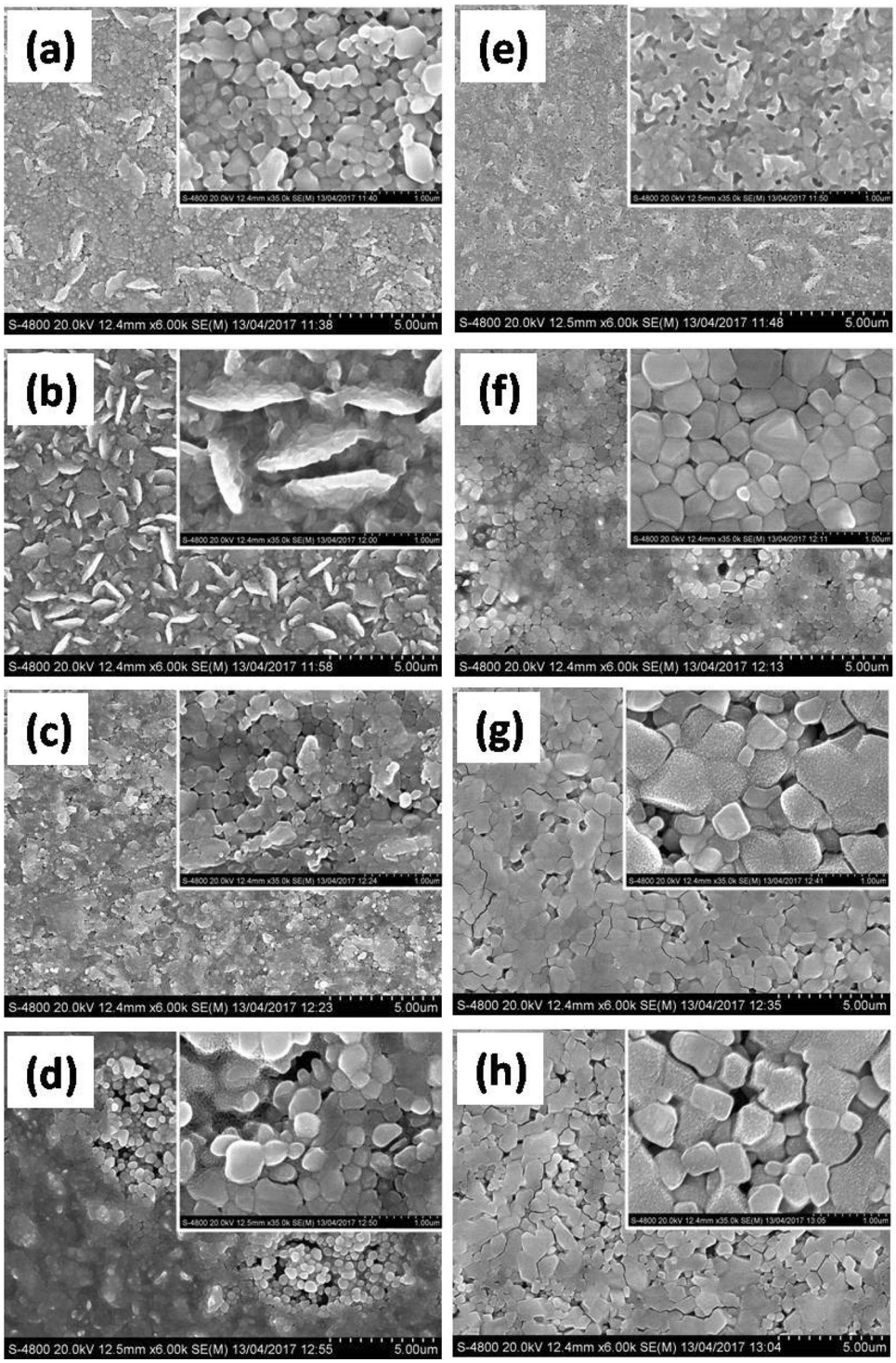


**Fig. 5** Scanning electron microscope images of the perovskite films deposited by two-step and three-step methods. **a**, **b**, **c** and **d** are films coated with two-step with 10 mg/ml, 20 mg/ml, 30 mg/ml and 40 mg/ml concentrations, respectively. **e**, **f**, **g** and **h** are films coated with three-step with 10 mg/ml, 20 mg/ml, 30 mg/ml and 40 mg/ml concentrations, respectively

seen. When the MAI concentration was increased to 20 mg/ml, density of the bigger flake-like structures increases in the film. With 30 mg/ml concentration of MAI, a compact film morphology is obtained with irregular shaped particles. In 40 mg/ml concentration, again compact films are obtained compared but with occasional porous spots and with bigger grain size. Films with three-step coating method are in general more compact and with less pores as compared to the two-step-coated films with same MAI concentration. With 10 mg/ml MAI concentration, better interconnected films are obtained compared to two-step film. With 20 mg/ml concentration, good quality film with less voids were obtained. With higher MAI concentrations the morphology was nearly same.

Raman spectroscopic measurements were performed for probing the effect of the MAI concentration on the organic-inorganic perovskite films. The excitation wavelength used in the present study is 633 nm, which is near resonance for Raman measurement of lead halide perovskite. As shown in Fig. 2, most intense peak corresponding to $PbI_2$ is at 113 $cm^{-1}$[27, 28]. The Raman spectra of formed perovskite films are shown in Fig. 6. For perovskite coated by two-step method the peaks are found at 74, 111, 138, 275 and at 355 $cm^{-1}$. Raman bands at 74 and 111 can be attributed to the stretching mode of Pb-I cage of perovskite $CH_3NH_3PbI_3$ [27, 29]. We attribute the band at 138 $cm^{-1}$ to libration mode of $MA^+$ cation and those at 275 $cm^{-1}$ and 355 $cm^{-1}$ can be assigned to the MA cation torsional mode of perovskite [29]. In 10 mg/ml MAI concentration film the intensity at 138 $cm^{-1}$ is much lower. This is in accordance with the XRD results, which shows incomplete transformation of $PbI_2$ into perovskite. The intensity however increases with MAI concentration and is maximum for 30 mg/ml MAI concentration film. In the films coated by three-step method with 20 mg/ml concentration the band intensity at 138 $cm^{-1}$ is maximum, which indicates better perovskite phase formation as compared to the film formed by using two-step method. XRD results also show minimum intensity at 12.7 and 11.6 values of $2\theta$ for film coated by three-step method with 20 mg/ml concentration. Upon increasing the MAI concentration further, the intensity corresponding to libration mode of $MA^+$ cation of perovskite decreases. This indicates that, in the third step the already formed perovskite (after the second step) is being washed away. This effect is more for the 40 mg/ml MAI concentration film. This is in accordance to the absorption spectra which shows a reduction in absorption. This also matches with the XRD studies, which show slight reduction in perovskite peak intensity.

The thickness and roughness values of the perovskite films have been shown in Table 2. It shows that for both two-step as well as three-step methods thickness of the film increases with MAI

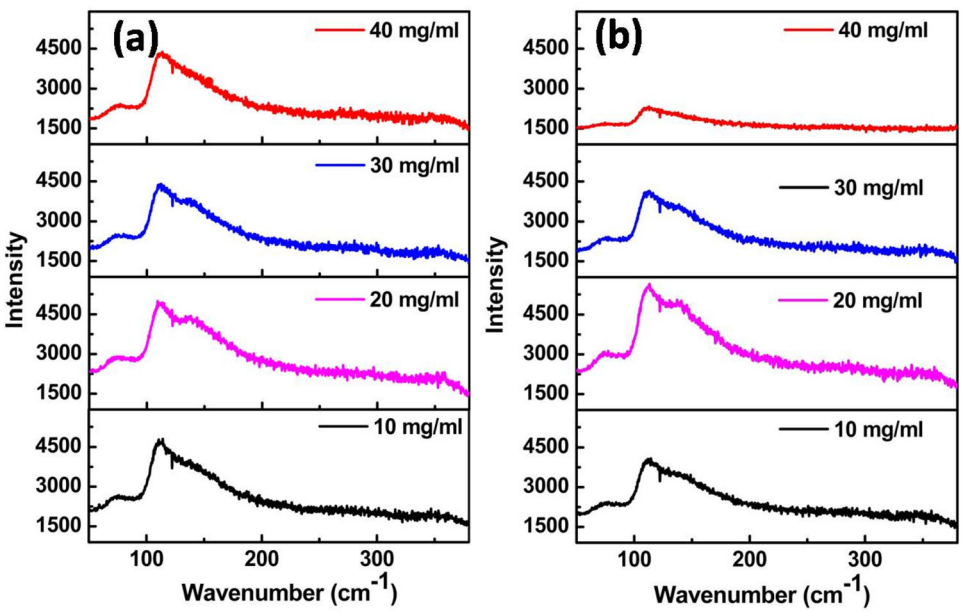


**Fig. 6** Raman spectra of the different perovskite films deposited by two- and three-step methods. **a** two-step method and **b** three-step method

**Table 2** Film thickness and roughness values of perovskite films are tabulated

| MAI concentration | Thickness (nm) | | Average roughness (nm) | |
|---|---|---|---|---|
| | Two-step | Three-step | Two-step | Three-step |
| 10 mg/ml | 310 | 315 | 90 | 91 |
| 20 mg/ml | 331 | 335 | 170 | 102 |
| 30 mg/ml | 342 | 410 | 200 | 125 |
| 40 mg/ml | 352 | 443 | 227 | 140 |

concentration. Thicknesses of films formed by three-step method are consistently greater than those formed with two-step method with same concentration. However, absorption coefficient of three-step films is not more than that of two-step films. This indicates that during the third step, some of the already formed perovskite is washed away and leaves some MAI in the film. Therefore, the thickness values obtained by profilometer are higher due to the excess MAI in the film especially for 30 mg/ml and 40 mg/ml films. Absorption as well as XRD studies have shown the presence of intercalated state of $PbI_2$ and MAI. The average roughness values also increases with increasing MAI concentration due to the formation of bigger crystals as shown earlier in the SEM images. Roughness values for the two-step and three-step films are nearly same at 10 mg/ml MAI concentration. At higher MAI concentration, the three-step film roughness values are lower as compared to the two-step films. This may be due to the presence of excess MAI in three-step films. Above discussion indicates better perovskite phase formation for 20 mg/ml MAI concentration using three-step method.

## 4 Conclusions

In conclusion, we have presented a comparative study of perovskite film properties formed by two-step and three-step sequential spin coating deposition techniques. Results show that at lower concentration of MAI, complete conversion of $PbI_2$ does not take place in two-step method. With increase in MAI concentration, however intercalated MAI into $PbI_2$ phase is formed. In three-step coating, good phase of perovskite and improved morphology is obtained at comparatively lower MAI concentration of 20 mg/ml. A higher concentration of MAI in three-step method leads to the removal of already formed perovskite material in the second step and leads to the formation of intercalated MAI and $PbI_2$. We show that the MAI concentration is very important factor in complete conversion of $PbI_2$ into the perovskite phase.

## Acknowledgements

Financial support from the CSR project (CSR-IC-265/2017-18/1346), Indore, India is acknowledged. SAM is thankful to UGC for RGNF.

## Compliance with ethical standards

**Conflict of interest** There are no conflicts to declare.

## References

1. Hannah Ritchie and Max Roser (2020) - "Fossil Fuels". *Published online at OurWorldInData.org*. Retrieved from: 'https://ourworldindata.org/fossil-fuels' [Online Resource]
2. P.A. Owusu, S. Asumadu-Sarkodie, Cogent Eng. **3**, 1–14 (2016)
3. E.D. Coyle, R.A. Simmons. Understanding the global energy crisis. Purdue University Press; 2014
4. K. Ranabhat, L. Patrikeev, A.A. evna Revina, K. Andrianov, V. Lapshinsky, E. Sofronova, J. Appl. Eng. Sci. **14**, 481–491 (2016)
5. Y. Zhao, C. Zhao, X. Chen, T. Luo, M. Ding, T. Ye, W. Zhang, H. Chang, J. Mater. Sci-Mater. El. **31**, 2167–2176 (2020)
6. I.K. Popoola, M.A. Gondal, T.F. Qahtan, Renew. Sustain. Energy Rev. **82**, 3127–3151 (2018)
7. J. Bahadur, A.H. Ghahremani, B. Martin, S. Pishgar, T. Druffel, M.K. Sunkara, K. Pal, J. Mater. Sci. Mater. Elec. (2019). https://doi.org/10.1007/s10854-019-02199-8
8. https://www.nrel.gov/pv/insights/assets/pdfs/cell-pv-eff-emergingpv.pdf (Accessed: 3rd April 2020)

9. K. Sim, T. Jun, J. Bang, H. Kamioka, J. Kim, H. Hiramatsu, H. Hosono, (2019) *Appl. Phys. Rev.* DOI: https://doi.org/10.1063/1.5098871
10. S.P. Senanayak, B. Yang, T.H. Thomas, N. Giesbrecht, W. Huang, E. Gann, B. Nair, K. Goedel, S. Guha, X. Moya, C.R. McNeill, P. Docampo, A. Sadhanala, R.H. Friend, H. Sirringhaus, Sci. Adv. **3**, 1–11 (2017)
11. M.M. Stylianakis, T. Maksudov, A. Panagiotopoulos, G. Kakavelakis, K. Petridis, Materials (Basel). **16**, 1–28 (2019)
12. J. Zhou, J. Huang, *Adv. Sci.* DOI:https://doi.org/10.1002/advs.201700256
13. T. Song, Q. Chen, H. Zhou, C. Jiang, H. Wang, M. Yang, Y. Liu, J. Mater. Chem. A Mater. Energy Sustain. **00**, 1–19 (2015)
14. E. Zheng, X.F. Wang, J. Song, L. Yan, W. Tian, T. Miyasaka, ACS Appl. Mater. Interfaces **7**, 18156–18162 (2015)
15. Z. Shi, A.H. Jayatissa, *Materials (Basel).*, 2018, 11
16. H. Zhou, Q. Chen, G. Li, S. Luo, T.B. Song, H.S. Duan, Z. Hong, J. You, Y. Liu, Y. Yang, Science. **345**, 542–546 (2014)
17. S.M. Jain, B. Philippe, E.M. Johansson, B.W. Park, H. Rensmo, T. Edvinsson, G.J. Boschloo, J. Mater. Chem. A. **4**, 2630–2642 (2016)
18. F. Yang, M.A. Kamarudin, P. Zhang, G. Kapil, T. Ma, S. Hayase, ChemSusChem **11**, 2348–2357 (2018)
19. D. Acuna, B. Krishnan, S. Shaji, S. Sepulveda, J.L. Menchaca, Bull. Mater. Sci. **39**, 1453–1460 (2016)
20. R.K. Misra, L. Ciammaruchi, S. Aharon, D. Mogilyansky, L. Etgar, I.V. Fisher, E.A. Katz, ChemSusChem **9**, 2572–2577 (2016)
21. H. Peng, Z. Su, Z. Zheng, H. Lan, J. Luo, P. Fan, G. Liang, Materials **12**, 1237 (2019)
22. S.M. Jain, B. Philippe, E.M.J. Johansson, B.W. Park, H. Rensmo, T. Edvinsson, G. Boschloo, J. Mater. Chem. A **4**, 2630 (2016)
23. D.H. Cao, C.C. Stoumpos, C.D. Malliakas, M.J. Katz, O.K. Farha, J.T. Hupp, M.G. Kanatzidis, APL Mater. **2**, 1–8 (2014)
24. P. Chhillar, B.P. Dhamaniya, V. Dutta, S.K. Pathak, ACS Omega **4**, 11880–11887 (2019)
25. G. Pellegrino, S. D'Angelo, I. Deretzis, G.G. Condorelli, E. Smecca, G. Malandrino, A. La Magna, A. Alberti, J. Phys. Chem. C **120**, 19768–19777 (2016)
26. C. Quarti, G. Grancini, E. Mosconi, P. Bruno, J.M. Ball, M.M. Lee, H.J. Snaith, A. Petrozza, F. De Angelis, J. Phys. Chem. Lett. **5**, 279–284 (2014)
27. W.M. Sears, M.L. Klein, J.A. Morrison, Phys. Rev. B **19**, 2305–2313 (1979)
28. R. Segovia, G. Qu, M. Peng, X. Sun, H. Shi, B. Gao, Nanoscale Res. Lett. **13**, 0–7 (2018)
29. R. Gottesman, L. Gouda, B.S. Kalanoor, E. Haltzi, S. Tirosh, E. Rosh-Hodesh, Y. Tischler, A. Zaban, C. Quarti, E. Mosconi, F. De Angelis, J. Phys. Chem. Lett. **6**, 2332–2338 (2015)